Experimental evidence for jump rope vortices in turbulent convective superstructures

Nayoung Kim
Institute of Fluid Dynamics, Helmholtz-Zentrum Dresden-Rossendorf, 01328 Dresden, Germany

Felix Schindler
Institute of Fluid Dynamics, Helmholtz-Zentrum Dresden-Rossendorf, 01328 Dresden, Germany

Sylvie Su
Institute of Fluid Dynamics, Helmholtz-Zentrum Dresden-Rossendorf, 01328 Dresden, Germany and CORIA–UMR 6614, Normandie Université, CNRS, INSA Rouen, 76800 Saint-Étienne-du-Rouvray, France

Sven Eckert*
Institute of Fluid Dynamics, Helmholtz-Zentrum Dresden-Rossendorf, 01328 Dresden, Germany

Tobias Vogt†
Institute of Fluid Dynamics, Helmholtz-Zentrum Dresden-Rossendorf, 01328 Dresden, Germany

(Received 17 February 2026; accepted 14 May 2026; published 30 June 2026)

We investigate turbulent Rayleigh-Bénard convection (RBC) in a convection cell with square cross section and aspect ratio $\Gamma = \text{width/height} = 25$ filled with the liquid metal alloy GaInSn at Prandtl number $Pr \approx 0.03$. A dense array of thermocouples and ultrasonic Doppler velocimetry is employed to measure the temperature distributions at the top of the convection cell and horizontal velocity profiles, respectively, in the Rayleigh number range $3.27 \times 10^4 \lesssim \mathrm{Ra} \lesssim 2.17 \times 10^5$. Conspicuous thermal structures manifest themselves in the two-dimensional temperature fields and closely resemble the turbulent superstructures predicted in numerical simulations. The velocity data reveal flow features that indicate the presence of "jump rope vortices" (JRV). This can be seen in characteristic oscillations that permeate the entire 3D flow structure. The measured frequencies, f_0 correspond very well with the empirical scaling $f_0 \propto \mathrm{Ra}^{0.419}$. The results thus provide experimental evidence that the jump-rope vortex, which has previously been identified as the striking dynamical feature of large-scale convection (LSC) in geometries with moderate aspect ratios ($1.4 \leqslant \Gamma \leqslant 5$), also persists as a robust, three-dimensional mode embedded within turbulent convective superstructures at very large aspect ratios.

DOI: 10.1103/653m-gc8d

*Contact author: s.eckert@hzdr.de
†Contact author: t.vogt@hzdr.de

Published by the American Physical Society under the terms of the Creative Commons Attribution 4.0 International license. Further distribution of this work must maintain attribution to the author(s) and the published article's title, journal citation, and DOI.

I. INTRODUCTION

Turbulent thermal convection organizes itself into coherent, system-spanning circulations that play a central role in global heat and momentum transport [1–5]. These large-scale circulations (LSCs) are a ubiquitous feature of convective systems and form the backbone of many geophysical and astrophysical flow phenomena [6–9]. Their structure and stability, however, depend sensitively on the lateral confinement of the system, commonly expressed by the aspect ratio $\Gamma = \text{width}/\text{height}$. For small aspect ratios, $\Gamma < 1$, multiple competing circulation rolls tend to coexist, leading to strongly unstable flow states. Recent experimental and numerical studies have connected these regimes to various instability mechanisms, including elliptical and shear-driven breakdown of coherent circulations [10–12]. In contrast, the widely studied case of $\Gamma \approx 1$ exhibits a comparatively robust single-roll LSC, whose low-dimensional dynamics can be described as a superposition of torsional and sloshing modes [13–17].

When the aspect ratio is increased beyond unity, this classical planar-roll picture breaks down [18–22]. LSC and flow structures in such systems have been extensively studied across a wide range of aspect ratios and parameter regimes [23–28]. For moderately wide containers ($1.4 \leqslant \Gamma \leqslant 5$), particularly in low-Prandtl-number convection, recent experimental and numerical work has identified a distinct three-dimensional oscillatory mode—the jump-rope vortex (JRV)—associated with the LSC [29–31]. In this state, the circulation adopts a precessing, ropelike trajectory reminiscent of a skipping rope, representing a nonlinear large-scale mode that extends beyond planar-roll descriptions. Remarkably, the JRV persists across different geometries within this regime, adapting its spatial organization while maintaining its characteristic precessing motion. At $\Gamma \approx 5$, for example, the flow can form synchronized networks of multiple interconnected JRVs [31].

This raises a fundamental question: Do such large-scale dynamics survive when the aspect ratio is increased by one order of magnitude and convection organizes itself into turbulent superstructures, or is this only a special phenomenon for a limited selection of geometries and aspect ratios? In sufficiently large aspect ratios, where the influence of the side walls vanishes, the flow develops long-lived patterns whose horizontal extent far exceeds the layer height [32–36]. Yet their connection to three-dimensional vortex dynamics such as the JRV remains unknown. Only a handful of direct numerical simulations have probed this regime, as the computational costs grow roughly with Γ^2 and the associated dynamical time scales require prohibitively long integration windows [32–34,36]. Experimental investigations at large Γ are even more scarce and do not exist for low Prandtl numbers.

II. EXPERIMENTAL SETUP

To approach this area of fluid dynamics, we constructed the *LIMECS* experiment at HZDR: a liquid-metal convection facility with an extreme aspect ratio of $\Gamma = 25$ (Fig. 1). The working fluid is the GaInSn liquid metal alloy that combines low viscosity and high thermal conductivity to a very low Prandtl number of $Pr \approx 0.03$. At such low Prandtl number, inertia dominates already at moderate Rayleigh numbers, resulting in strongly fluctuating, turbulence-dominated flows with large thermal diffusivity and therefore moderate Péclet numbers. As a consequence, temperature fields remain coherent on system scales despite intense velocity fluctuations, amplifying periodic flow signatures and enabling the detection of subtle dynamical modes in turbulent convection.

In this paper, we present experimental evidence that JRVs persist as one of the prominent dynamical features within turbulent superstructures at extreme aspect ratios. Our results demonstrate that the jump-rope mode survives far beyond previously explored geometries, indicating that it constitutes a fundamental organizing mechanism of turbulent convection. Beyond the laboratory, our results may offer guidance for interpreting flow organization in large, weakly confined convection layers in geophysical and astrophysical systems, including the highly dynamic nature of solar granulation [37].

The experiments were conducted in a convection cell of aspect ratio $\Gamma = 25$ with a square cross section of 1 m^2 and height $H = 40$ mm (Fig. 1). Thermal forcing was applied through temperature-

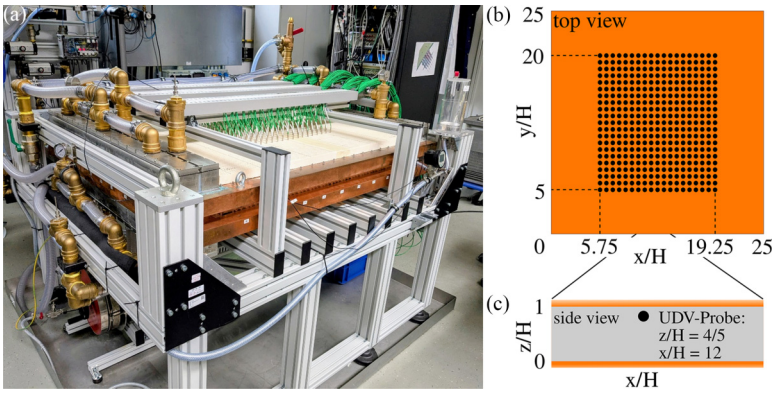


FIG. 1. Photograph of the experiment (a) and schemata of the sensor positions on the top plate (b) and on the side wall (c). The Rayleigh-Bénard convection cell with aspect ratio $\Gamma = 25$ contains the liquid metal GaInSn, enclosed between temperature-controlled copper plates that provide uniform thermal boundary conditions. UDV sensors are mounted on the sidewalls, and a dense thermocouple array is embedded in the top copper plate at a distance of 2 mm from the fluid-facing surface, while a smaller number of thermocouples are installed in the bottom plate for measuring the mean temperature difference.

controlled copper plates, heated and cooled by independent thermostats with capacities up to 100 kW, and water maintained at a temperature stability within ± 0.1 K. The temperature-control channels embedded in the copper plates were designed and optimized using COMSOL simulations to achieve spatially homogeneous, but not strictly isothermal, boundary conditions. Due to the large heat transport inherent to liquid-metal Rayleigh-Bénard convection, perfectly isothermal plates are neither feasible nor required. Instead, the design minimizes lateral temperature variations within the plates while allowing for finite temperature fluctuations induced by the turbulent flow. Temperature variations associated with turbulent superstructures were monitored using thermocouples embedded within the copper plates at a distance of 2 mm from the fluid-facing surfaces. The thermocouple array was sampled at a time interval of 3 s. In particular, the top plate contained 21×19 sensors arranged in a dense grid, enabling spatially and temporally resolved measurements of the temperature field imprinted by the large-scale flow organization. The bottom plate held 25 sensors used primarily to determine the mean temperature difference for calculating the Rayleigh number, $\mathrm{Ra} = g\alpha\Delta T H^3/(\nu\kappa)$, where g is the gravitational acceleration, α the thermal expansion coefficient, and ΔT the temperature difference between plates. The present experiments reached values up to $\mathrm{Ra} = 2.17 \times 10^5$. Horizontal velocity profiles were simultaneously measured by ultrasound Doppler velocimetry (UDV) using transducers installed at the sidewalls. While several probes were available, the analysis presented here focuses on selected measurement lines that capture the dominant large-scale oscillatory dynamics. In addition, two UDV probes mounted on opposite sidewalls were used, and their one-dimensional velocity profiles were combined to reconstruct the velocity field over the full extent of the measurement domain.

III. RESULTS

Before addressing the dynamical nature of the large-scale flow, we first establish that the present $\Gamma = 25$ experiment operates in the regime of turbulent superstructures. Figure 2(a) shows the time-averaged normalized temperature fluctuations measured inside the top plate at $\mathrm{Ra} = 2.17 \times 10^5$ near the top boundary layer. The field was reconstructed from a grid of 21×19 thermocouples [see Fig. 1(b)]. The resulting map was averaged over $27\,t_{ff}$, where $t_{ff} = \sqrt{H/(g\alpha\Delta T)} = 1.95$ s is the free-fall time that represents the inertial response time of the flow to buoyancy forcing and sets the natural advective time scale in buoyancy-driven turbulence. The resulting field exhibits an extended

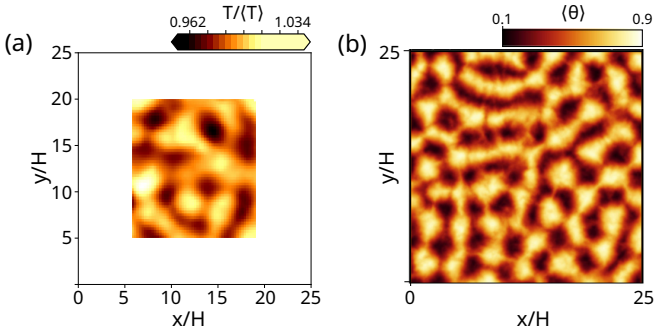


FIG. 2. (a) Time-averaged temperature field $T/\langle T\rangle$ normalized by the average of each sensor over the whole measurement time $\langle T\rangle$. After normalization, the data from the 21×19 thermocouples were averaged over a window of 27 t_{ff} and polynomially interpolated onto a 50×50 grid for visualization. The applied Rayleigh number is $\mathrm{Ra} = 2.17 \times 10^5$. (b) Time-averaged midplane temperature field $\langle\theta\rangle$ from direct numerical simulation at $\mathrm{Ra} = 10^5$ and $Pr = 0.021$, reproduced from Pandey *et al.* [33], licensed under CC BY 4.0. Here $\theta = T - T_{\mathrm{lin}}(z)$ is the deviation from the linear conductive profile, and $\langle\theta\rangle$ denotes its time average over $27\,t_{ff}$.

cellular temperature pattern with lateral length scales that exceed the layer height significantly. These structures persist over many free-fall times and therefore represent slow changing features of the flow rather than transient plume dynamics. To verify that these patterns correspond to turbulent superstructures previously identified in numerical studies, we compare our experimental temperature field to the midplane temperature distribution obtained from direct numerical simulations by Pandey *et al.* [33], shown in Fig. 2(b). Despite important differences—most notably the probing height (near the top boundary in the experiment versus midheight in the DNS) and the slightly different Rayleigh and Prandtl numbers—the overall morphology and characteristic lateral scales are similar. In both cases, the flow organizes into a cellular arrangement of alternating warm and cold regions.

The marginal discrepancies can be attributed to the fact that near-wall measurements at low Prandtl numbers are more dominated by plume emission and flow-influenced boundary-layer dynamics while midplane fields reflect mainly the bulk circulation [38,39]. Nevertheless, the similarities confirm that the present liquid-metal experiment realizes the turbulent superstructure regime and provides a suitable framework for investigating the underlying large-scale flow dynamics.

We now focus on the horizontal velocity field and its relation to known large-scale circulation modes. Figure 3(a) shows the jump-rope vortex (JRV) network in Rayleigh-Bénard convection via phase-averaged streamlines from direct numerical simulations at aspect ratio $\Gamma = 5$ [31]. The color scale represents the vertical velocity component u_z (blue/red for downward/upward flow). The streamlines reveal four interlaced JRVs whose ends cross perpendicularly at specific locations. Figures 3(c) and 3(d) display spatiotemporal plots of the horizontal velocity components u_x and u_y for a comparable experimental configuration in $\Gamma = 5$. The $\Gamma = 5$ data are taken from a separate experimental dataset obtained using a different setup, and are included here for comparison with the present $\Gamma = 25$ measurements. The characteristic inclined bands and alternating velocity signs reflect the precessing motion of the jump-rope vortex cores, which generates antisymmetric horizontal velocities oscillating coherently throughout the cell. This oscillatory signature is a robust experimental fingerprint of JRV dynamics.

Accordingly, the corresponding measurements for $\Gamma = 25$, shown in Figs. 3(e) and 3(f), reveal coherent oscillatory patterns that extend across the measurement domain. These include inclined spatiotemporal velocity bands and alternating horizontal velocity components, indicating antisymmetric flow oscillations throughout the cell. Despite the much larger lateral extent and the strongly reduced stabilizing influence of the sidewalls, these features persist across the measurement domain.

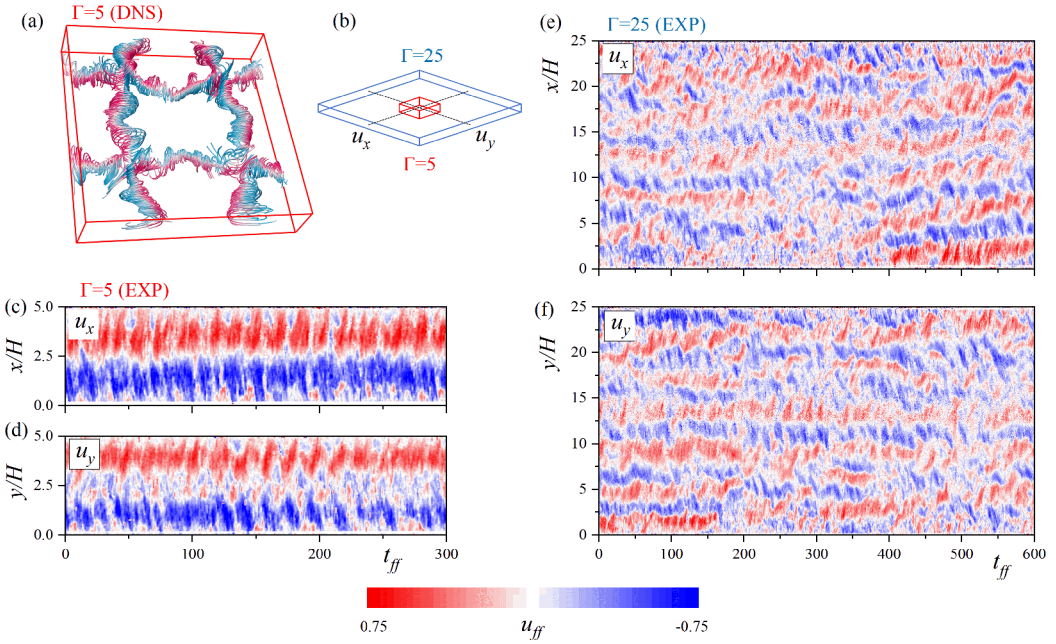


FIG. 3. (a) Visualization of the jump rope vortex (JRV) network in a $\Gamma = 5$ container at $\mathrm{Pr} = 0.03$ and $\mathrm{Ra} = 10^6$, from DNS by Teimurazov *et al.* [31], available under CC BY-NC-ND 4.0. (b) Schematic of the experimental setups for $\Gamma = 5$ and $\Gamma = 25$, showing UDV measurement lines for u_x and u_y. (c), (d) Spatiotemporal distribution of the experimentally measured dimensionless horizontal velocities u_x/u_{ff} and u_y/u_{ff} at $z/H = 0.75$ and $\mathrm{Ra} = 2.2 \times 10^5$ for $\Gamma = 5$, displaying oscillations characteristic of JRV motion. (e), (f) Corresponding diagrams for $\Gamma = 25$ at $\mathrm{Ra} = 2.4 \times 10^5$ reveal large-scale, periodic oscillations of similar frequency and spatial scale, indicative of JRV dynamics within the superstructure regime.

While a full three-dimensional reconstruction is not possible with the present measurements, the observed spatiotemporal velocity signatures are consistent with experimentally established fingerprints of JRV dynamics.

At the same time, notable differences emerge. Compared to the $\Gamma = 5$ case, the patterns in the $\Gamma = 25$ cell are less regular and are superimposed by additional spatiotemporal variability. This increased complexity reflects the substantially higher number of degrees of freedom in the wide cell. With diminished lateral confinement, convection cells are no longer anchored to the sidewalls but can drift and reorganize, leading to a superposition of JRV dynamics with additional large-scale motions. The crucial point, however, is that the oscillatory signal itself remains clearly identifiable and retains the same characteristic spatiotemporal structure as in confined geometries.

If the oscillatory mode observed in the $\Gamma = 25$ system corresponds to a jump-rope vortex, its characteristic lateral wavelength and oscillation frequency should be consistent with those previously reported for JRVs in smaller-aspect-ratio systems. While the available Rayleigh number range limits a direct scaling analysis of the wavelength, a quantitative comparison of its magnitude nevertheless provides a stringent consistency check.

Figure 4 shows the dominant horizontal wavelength λ/H extracted from the UDV velocity fields as a function of the Rayleigh number. The characteristic wavelength is extracted from the UDV velocity fields using a spatial Fourier transform along the measurement direction (y/H). The resulting power spectra are averaged over time, and the dominant wavelength is determined from the peak wavenumber of the averaged spectrum as $\lambda = 1/k$. Prior to the Fourier transform, the data are windowed and slightly trimmed near the boundaries to reduce edge effects. The peak position is further refined using a quadratic interpolation around the spectral maximum. The uncertainty

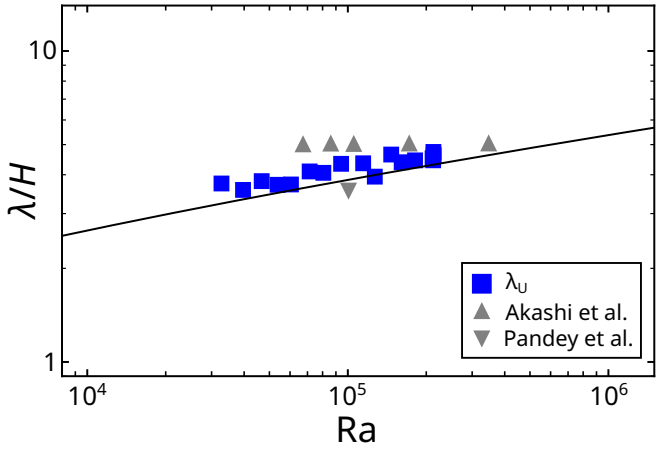


FIG. 4. Dimensionless horizontal wavelength λ/H as a function of the Rayleigh number, extracted from the oscillatory mode of the horizontal velocity field. Blue symbols denote the present experimental data for flow states exhibiting clear jump-rope vortex signatures, while the other symbols correspond to values reported in previous studies by Akashi *et al.* [40] and Pandey *et al.* [33]. The data from Pandey *et al.* correspond to measurements in the turbulent superstructure regime, where no explicit identification of oscillatory large-scale modes was performed. The solid line indicates the empirical relation $\lambda/H = 1.85\,\mathrm{Ra}^{0.10} - 2$ reported in Ref. [40], obtained from a broad range of flow regimes and shown here for reference.

in the wavelength is associated with the finite spectral resolution of the Fourier transform and is estimated as $\Delta\lambda = \frac{1}{2}\,\Delta\lambda_{\mathrm{bin}}$, where $\Delta\lambda_{\mathrm{bin}}$ denotes the wavelength interval corresponding to one Fourier wavenumber bin. This uncertainty is smaller than the marker size in Fig. 4. Although the accessible range of Rayleigh numbers is too limited to extract a reliable scaling exponent, the measured wavelengths are consistent with the characteristic lateral length scale of the cellular flow pattern reported previously for $\Gamma = 5$ Rayleigh-Bénard convection [40], which is known to be formed by a JRV network [30,31]. Notably, the characteristic wavelength reported by Pandey *et al.* [33], who investigated the same turbulent superstructure regime without identifying specific large-scale oscillatory modes, agrees closely with the wavelength of the oscillatory mode observed here. This suggests that the jump-rope vortex dynamics develop on the intrinsic lateral length scale set by turbulent superstructures. For reference, the solid line indicates the empirical relation

$$\lambda/H = 1.85\,\mathrm{Ra}^{0.10} - 2,$$

which was obtained from studies spanning a broad range of flow regimes, including roll-dominated convection at lower Rayleigh numbers [40]. This empirical relation was proposed by Akashi *et al.* [40] based on a compilation of data from multiple previous studies spanning different flow regimes. We note that in the original experiments of Akashi *et al.* at $\Gamma = 5$, the characteristic wavelength exhibits only weak dependence on the control parameters, as the lateral extent of the convective structures is constrained by the finite system size. The measured wavelengths fall within a similar range, indicating that the intrinsic lateral scale of the oscillatory mode observed here is comparable to previously reported large-scale convective structures, even in the turbulent superstructure regime and at extreme aspect ratio. We emphasize that this comparison is intended as a consistency check in magnitude, rather than as a validation of the empirical scaling in the present regime. While the wavelength comparison establishes geometric consistency with previously reported large-scale convective length scales, the oscillation frequency provides a more stringent test of the underlying dynamics.

Figure 5 displays the nondimensional oscillation frequency fH^2/κ obtained from the dominant coherent mode of the UDV signal. The characteristic frequency is extracted from the UDV signals

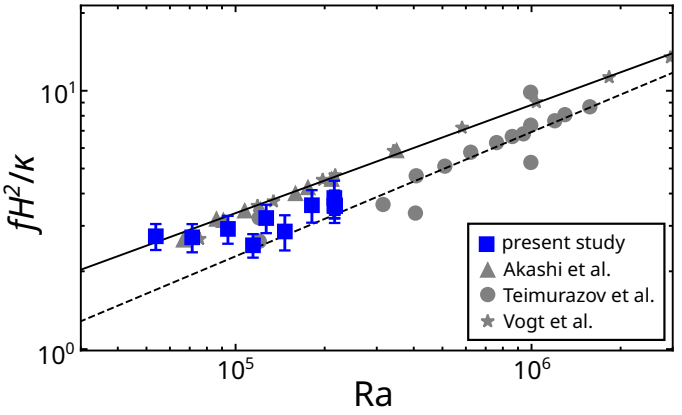


FIG. 5. Nondimensional oscillation frequency fH^2/κ as a function of the Rayleigh number. Blue symbols represent the present experimental data obtained from UDV measurements at $z/H = 0.75$, while the other symbols correspond to results from previous studies by Akashi *et al.* [30], Teimurazov *et al.* [31], and Vogt *et al.* [29]. The solid line indicates the empirical scaling $fH^2/\kappa = 0.027\,\mathrm{Ra}^{0.419}$ from Ref. [29], while the dashed line represents the scaling $fH^2/\kappa = 0.009\,\mathrm{Ra}^{0.481}$ from Ref. [31].

using a short-time Fourier transform (STFT). The dominant oscillatory mode is identified from the ridge of the time-frequency spectrum, and the characteristic frequency is defined as the median value of the instantaneous ridge frequency over time. The associated uncertainty is quantified from the temporal variability of the ridge frequency, expressed as half of the interquartile range (IQR). In contrast to the wavelength, the frequency data span a sufficiently broad Rayleigh number range to allow for a direct scaling analysis. The $\Gamma = 25$ data collapse remarkably onto the established jump-rope vortex scaling law

$$fH^2/\kappa \sim \mathrm{Ra}^{0.419},$$

originally identified for JRVs in a confined cylindrical geometry with $\Gamma = 2$ [29] and subsequently examined in both experiments and numerical simulations at comparable aspect ratios ($\Gamma = 2 - 5$) [31], where a slightly steeper scaling, $fH^2/\kappa = 0.009\,\mathrm{Ra}^{0.481}$, was also reported. The close agreement over more than a fivefold increase in aspect ratio provides strong evidence that the same physical mechanism governs the oscillatory dynamics in these systems.

Taken together, the consistency of the measured wavelength with established large-scale convective length scales, combined with the collapse of the oscillation frequency onto the JRV-specific scaling, provides quantitative confirmation that the oscillations observed within turbulent superstructures correspond to genuine jump-rope vortex dynamics. The JRV thus persists as a robust three-dimensional mode even when the large-scale circulation is embedded in a spatially extended, weakly confined superstructure. These results suggest that JRV dynamics are not restricted to confined geometries, but can persist within turbulent superstructures at large aspect ratio. This points to a closer connection between large-scale circulation in confined systems and the superstructure regime in extended domains, indicating that similar mechanisms may govern the spatiotemporal organization of convection across a wide range of geometries.

IV. CONCLUSIONS

In summary, we have presented experimental evidence that the jump-rope vortex persists within turbulent convective superstructures at extreme aspect ratio. Using a liquid-metal Rayleigh-Bénard experiment with $\Gamma = 25$ and $Pr \approx 0.03$, we demonstrated that the flow organizes into turbulent superstructures whose thermal signatures closely resemble those reported in large-aspect-ratio nu-

merical simulations. Horizontal velocity measurements revealed characteristic oscillatory patterns that qualitatively and quantitatively coincide with known JRV dynamics from smaller aspect-ratio systems.

The central finding of this work is that the jump-rope vortex remains a robust structural element of turbulent convection even in extended domains with weak lateral confinement. Our results suggest that JRVs act as fundamental three-dimensional building blocks that are embedded within, and potentially organize, turbulent superstructures. Given that similar oscillatory JRV dynamics have also been observed in small aspect ratios at higher Prandtl numbers, albeit with reduced amplitudes, we expect this mechanism to be generic across a wide range of convective systems.

These findings may have implications for geophysical and astrophysical convection, where flows typically occur in laterally extended layers with minimal confinement. In such systems, jump-rope–like vortex dynamics may contribute to the organization and temporal modulation of large-scale convective patterns.

ACKNOWLEDGMENTS

We gratefully acknowledge Klaus Timmel for his valuable support in the design and construction of the experimental facility. This work was supported by the Deutsche Forschungsgemeinschaft (DFG) within the Priority Programme SPP 1881 "Turbulent Superstructures" under Grant No. VO 2331/3, and by the DFG under Grant No. EC 217/5-1.

DATA AVAILABILITY

The data supporting the findings shown in Figs. 4 and 5 are openly available in Ref. [41].

[1] G. Zocchi, E. Moses, and A. Libchaber, Coherent structures in turbulent convection, an experimental study, Physica A **166**, 387 (1990).

[2] X.-L. Qiu, S.-H. Yao, and P. Tong, Large-scale coherent rotation and oscillation in turbulent thermal convection, Phys. Rev. E **61**, R6075 (2000).

[3] X.-L. Qiu and P. Tong, Onset of coherent oscillations in turbulent Rayleigh–Bénard convection, Phys. Rev. Lett. **87**, 094501 (2001).

[4] T. Hartlep, A. Tilgner, and F. H. Busse, Large scale structures in Rayleigh–Bénard convection at high Rayleigh numbers, Phys. Rev. Lett. **91**, 064501 (2003).

[5] J. Von Hardenberg, A. Parodi, G. Passoni, A. Provenzale, and E. Spiegel, Large-scale patterns in Rayleigh–Bénard convection, Phys. Lett. A **372**, 2223 (2008).

[6] R. Krishnamurti and L. N. Howard, Large-scale flow generation in turbulent convection, Proc. Natl. Acad. Sci. USA **78**, 1981 (1981).

[7] T. Hartlep, A. Tilgner, and F. H. Busse, Transition to turbulent convection in a fluid layer heated from below at moderate aspect ratio, J. Fluid Mech. **544**, 309 (2005).

[8] J. Aurnou, M. Calkins, J. Cheng, K. Julien, E. King, D. Nieves, K. M. Soderlund, and S. Stellmach, Rotating convective turbulence in Earth and planetary cores, Phys. Earth Planet. Inter. **246**, 52 (2015).

[9] P. P. Vieweg, J. D. Scheel, and J. Schumacher, Supergranule aggregation for constant heat flux-driven turbulent convection, Phys. Rev. Res. **3**, 013231 (2021).

[10] K. P. Iyer, J. D. Scheel, J. Schumacher, and K. R. Sreenivasan, Classical 1/3 scaling of convection holds up to Ra = 1015, Proc. Natl. Acad. Sci. USA **117**, 7594 (2020).

[11] L. Zwirner, A. Tilgner, and O. Shishkina, Elliptical instability and multiple-roll flow modes of the large-scale circulation in confined turbulent Rayleigh–Bénard convection, Phys. Rev. Lett. **125**, 054502 (2020).

[12] F. Schindler, S. Eckert, T. Zürner, J. Schumacher, and T. Vogt, Collapse of coherent large scale flow in strongly turbulent liquid metal convection, Phys. Rev. Lett. **128**, 164501 (2022).

[13] E. Brown and G. Ahlers, The origin of oscillations of the large-scale circulation of turbulent Rayleigh–Bénard convection, J. Fluid Mech. **638**, 383 (2009).
[14] D. Funfschilling and G. Ahlers, Plume motion and large-scale circulation in a cylindrical Rayleigh–Bénard cell, Phys. Rev. Lett. **92**, 194502 (2004).
[15] Q. Zhou, H.-D. Xi, S.-Q. Zhou, C. Sun, and K.-Q. Xia, Oscillations of the large-scale circulation in turbulent Rayleigh–Bénard convection: The sloshing mode and its relationship with the torsional mode, J. Fluid Mech. **630**, 367 (2009).
[16] H.-D. Xi, S.-Q. Zhou, Q. Zhou, T.-S. Chan, and K.-Q. Xia, Origin of the temperature oscillation in turbulent thermal convection, Phys. Rev. Lett. **102**, 044503 (2009).
[17] T. Zürner, F. Schindler, T. Vogt, S. Eckert, and J. Schumacher, Combined measurement of velocity and temperature in liquid metal convection, J. Fluid Mech. **876**, 1108 (2019).
[18] X. Xu, K. M. Bajaj, and G. Ahlers, Heat transport in turbulent Rayleigh–Bénard convection, Phys. Rev. Lett. **84**, 4357 (2000).
[19] S. Horn, P. J. Schmid, and J. M. Aurnou, Unravelling the large-scale circulation modes in turbulent Rayleigh–Bénard convection, Europhys. Lett. **136**, 14003 (2021).
[20] J. S. Cheng, I. Mohammad, B. Wang, D. F. Keogh, J. M. Forer, and D. H. Kelley, Oscillations of the large-scale circulation in experimental liquid metal convection at aspect ratios 1.4–3, J. Fluid Mech. **949**, A42 (2022).
[21] O. Shishkina, Rayleigh–Bénard convection: The container shape matters, Phys. Rev. Fluids **6**, 090502 (2021).
[22] R. J. Stevens, R. Hartmann, R. Verzicco, and D. Lohse, How wide must Rayleigh–Bénard cells be to prevent finite aspect ratio effects in turbulent flow? J. Fluid Mech. **1000**, A58 (2024).
[23] X.-L. Qiu and P. Tong, Large-scale velocity structures in turbulent thermal convection, Phys. Rev. E **64**, 036304 (2001).
[24] R. Du Puits, C. Resagk, and A. Thess, Breakdown of wind in turbulent thermal convection, Phys. Rev. E **75**, 016302 (2007).
[25] J. Bailon-Cuba, M. S. Emran, and J. Schumacher, Aspect ratio dependence of heat transfer and large-scale flow in turbulent convection, J. Fluid Mech. **655**, 152 (2010).
[26] E. P. van der Poel, R. J. Stevens, K. Sugiyama, and D. Lohse, Flow states in two-dimensional Rayleigh-Bénard convection as a function of aspect-ratio and Rayleigh number, Phys. Fluids **24**, 085104 (2012).
[27] P. Sakievich, Y. Peet, and R. Adrian, Large-scale thermal motions of turbulent Rayleigh–Bénard convection in a wide aspect-ratio cylindrical domain, Int. J. Heat Fluid Flow **61**, 183 (2016).
[28] Y.-Z. Li, X. Chen, A. Xu, and H.-D. Xi, Counter-flow orbiting of the vortex centre in turbulent thermal convection, J. Fluid Mech. **935**, A19 (2022).
[29] T. Vogt, S. Horn, A. M. Grannan, and J. M. Aurnou, Jump rope vortex in liquid metal convection, Proc. Natl. Acad. Sci. USA **115**, 12674 (2018).
[30] M. Akashi, T. Yanagisawa, A. Sakuraba, F. Schindler, S. Horn, T. Vogt, and S. Eckert, Jump rope vortex flow in liquid metal Rayleigh–Bénard convection in a cuboid container of aspect ratio, J. Fluid Mech. **932**, A27 (2022).
[31] A. Teimurazov, S. Singh, S. Su, S. Eckert, O. Shishkina, and T. Vogt, Oscillatory large-scale circulation in liquid-metal thermal convection and its structural unit, J. Fluid Mech. **977**, A16 (2023).
[32] R. J. A. M. Stevens, A. Blass, X. Zhu, R. Verzicco, and D. Lohse, Turbulent thermal superstructures in Rayleigh–Bénard convection, Phys. Rev. Fluids **3**, 041501(R) (2018).
[33] A. Pandey, J. D. Scheel, and J. Schumacher, Turbulent superstructures in Rayleigh–Bénard convection, Nat. Commun. **9**, 2118 (2018).
[34] G. Green, D. G. Vlaykov, J. P. Mellado, and M. Wilczek, Resolved energy budget of superstructures in Rayleigh–Bénard convection, J. Fluid Mech. **887**, A21 (2020).
[35] D. Krug, D. Lohse, and R. J. Stevens, Coherence of temperature and velocity superstructures in turbulent Rayleigh–Bénard flow, J. Fluid Mech. **887**, A2 (2020).
[36] A. Pandey, D. Krasnov, K. R. Sreenivasan, and J. Schumacher, Convective mesoscale turbulence at very low Prandtl numbers, J. Fluid Mech. **948**, A23 (2022).

[37] Å. Nordlund, R. F. Stein, and M. Asplund, Solar surface convection, Living Rev. Sol. Phys. **6**, 1 (2009).
[38] N. Kim, F. Schindler, T. Vogt, and S. Eckert, Thermal boundary layer dynamics in low-Prandtl-number Rayleigh–Bénard convection, J. Fluid Mech. **994**, A4 (2024).
[39] F. Schindler, N. Kim, T. Vogt, and S. Eckert, Impact of fluid flow on the thermal boundary layer dynamics in turbulent liquid metal Rayleigh–Bénard convection, Int. J. Heat Mass Transf. **247**, 127129 (2025).
[40] M. Akashi, T. Yanagisawa, Y. Tasaka, T. Vogt, Y. Murai, and S. Eckert, Transition from convection rolls to large-scale cellular structures in turbulent Rayleigh–Bénard convection in a liquid metal layer, Phys. Rev. Fluids **4**, 033501 (2019).
[41] N. Kim, F. Schindler, S. Su, S. Eckert, and T. Vogt, Experimental evidence for jump rope vortices in turbulent convective superstructures [Data set], Rodare, 2026, http://doi.org/10.14278/rodare.4663.